

THE IDENTIFICATION OF FAILURE INITIATION HOTSPOTS IN IDEALISED COMPOSITE MATERIAL COMPONENT MODELS USING A “BOTTOM-UP DATABASE” METHOD

X. Zou^{*1}, S. Yan¹, J. Rouse², M. Matveev¹, S. Li¹, I. A. Jones¹, M. Hamadi³, M. Fouinneteau³

¹Composites Research Group, Faculty of Engineering, University of Nottingham, Nottingham, NG7 2RD, United Kingdom

²Gas Turbine and Transmission Research Centre (G2TRC), Faculty of Engineering, University of Nottingham, Nottingham, NG7 2TU, United Kingdom

³Airbus Operations S.A.S., 316 Route de Bayonne, Toulouse, 31300, France

* Email: xi.zou@nottingham.ac.uk

Keywords: multiscale modelling, laminates, finite element analysis, failure initiation, delamination

Abstract

Idealisations are inevitable for finite element simulations of complex composite structures especially airframes, where laminates are commonly modelled using shell elements for relatively low computational cost. However, identification of failure initiation locations is crucial in designing airworthy structures, which requires complex models incorporating details to capture damage initiation accurately. This often leads to high computational cost and is only acceptable in sub-models for some local regions of interest. In this work, we present a method for re-using results of detailed models to identify failure initiation hotspots in global models. In the workflow, commonly encountered geometric features are analysed in isolation from complex structures. Unit loads are applied individually to a detailed feature model, wherein stresses at critical points are extracted and stored in a database, which will be later accessed to identify failure initiation hotspots by testing interface loads extracted at feature boundaries of the global model against the developed database. This workflow is demonstrated with an L-shaped clip model. Comments and discussions on modelling errors are also presented regarding the confidence in hotspot location predictions. This approach is considered more efficient than traditional ones for components with a limited number of common features.

1. Introduction

Some level of idealisation and simplification of complex heterogeneous structures is inevitable in finite element analyses (FEA) of composite components. This is particularly true for the analysis of composite materials in airframes, wherein laminates are commonly modelled using shells and some geometric features, such as bolt and rivet connections, are rationalised as simple constraints placed on the model. This methodology makes it possible to predict the (elastic) response of a structure accurately and within a relatively short computational time.

However, estimation of the loads leading to the damage initiation and propagation is also required for the design of an airworthy structure. While some damage mechanisms, such as fibre failure, can be potentially estimated using models based on thin shells [1], other damage mechanisms, such as delamination, require multi-scale 3D models with *ad hoc* techniques such as cohesive zone models (CZM) [2, 3] and/or the extended finite element method (XFEM) [4–6] to properly capture damage initiation and growth between the bonded layers. Those methods are often integrated with *a priori* damage criteria

and intrusive numerical implementations. Obviously, owing to the computation costs, the use of such modelling approaches is infeasible for analysis of an entire component but can be used in a sub-modelling or “dive-deeper” procedures [7] for a limited number of regions of interest.

Jansen *et al.* [8, 9] demonstrated the potential of a two-way loose coupling global-local finite element (FE) approach for the progressive failure analysis for large stiffened panels. Specifically, the term “two-way” or “one-way” indicates the information transfer between global and local models. In this present work, a simplified but more general one-way method is presented that allows the results of independent detailed models to be used to judge the likelihood of a failure initiation site, here referred to as a “hotspot”, being encountered in a simplified shell element model. In the proposed workflow, commonly encountered simple geometric features are modelled in detail, involving CZM and analysed in isolation from any potential structure. Unit loads are applied individually to predefined degrees of freedom and stress tensors at presumed critical points in the structure are extracted. These stress responses are scaled and combined (in accordance with linear superposition) in order to identify loading combinations that potentially lead to failure by one of several damage mechanisms, and eventually form a failure database. Interface loads at the assumed boundary of the feature can be extracted from the global simplified model and tested against the developed bottom-up database. Crucially, an empirical assumption is made that the global model material can be considered linear elastic for the onset of failure to be estimated.

The proposed workflow is demonstrated via the analysis of an L-shaped clip under four-point bending test. This shape contains one of the most common features in large aerospace subcomponent models (for example stringers and rib sections), and is usually modelled as a curved laminated beam and is extensively investigated in the literature [10–14]. The analysis results are compared to high-fidelity models to illustrate the accuracy of the proposed approach. Comments on errors related to the modelling procedure are also presented and methods are discussed that use this information to provide confidence in hotspot location predictions. The proposed workflow is considered to be a more efficient than simple dive-deeper approach for components with a limited number of features that are specified based on set design rules.

2. Materials and Methods

For most engineering structure analyses, global input and output variables and their relationships are mostly of interest, whilst the detailed physical mechanism, although it sometimes dominates the macroscopic behaviour, is not so much the main focus. An example study on the L-shaped clip under four-point bending load is detailed in this section, following previous studies by Charrier *et al.* [13]. The curved laminated beam specimens are manufactured with 32 plies of T700GC/M21 UD prepreg lamina with a highly oriented stack sequence $[0^{\circ}_3/45^{\circ}/90^{\circ}_2/135^{\circ}/0^{\circ}]_{2s}$. The mechanical properties of a single ply are listed in Table 1, with the nominal ply thickness assumed at 0.262 mm and transversal width W selected at 40 mm. The two arms are nominally perpendicular to each other at the initial configuration. Following standard [15], the experimental settings to be modelled are illustrated in Figure 1, and the geometric parameters regarding the specimen and experimental settings are reported in Table 2. In this case, the quantity of interest is the applied load P under which the damage failure initiates. According to *a priori* knowledge, it is known that the potential critical region lies on the curved fillet of the L-shaped specimen. Therefore, the curved location is considered a feature of this component and will be focused on under the proposed workflow.

To implement the workflow, Abaqus/Standard is selected as the FEA solver. Due to its thickness, the specimen is meshed with C3D8R solid elements in both high-fidelity global and feature models. The support rollers are assumed to be rigid, and are modelled with analytical rigid bodies. Frictionless contact is defined between specimen and support rollers, and non-linearities due to large displacements are taken

into account.

Table 1. Material properties of T700GC/M21 UD prepreg ply.

| E_{11} (MPa) | E_{22} (MPa) | ν_{12} | ν_{23} | G_{12} (MPa) |
|----------------|----------------|------------|------------|----------------|
| 115 000 | 8400 | 0.32 | 0.4 | 4500 |

Table 2. Nominal dimensions of L-shaped clip and characteristic parameters for four-point bending test.

| Thickness t (mm) | Length L (mm) | Width W (mm) | Inner radius R_i (mm) | Roller radius R_r (mm) | Roller distance 1 X_1 (mm) | Roller distance 2 X_2 (mm) |
|-----------------------|--------------------|-------------------|----------------------------|-----------------------------|---------------------------------|---------------------------------|
| 8.38 | 72 | 40 | 8 | 7.5 | 42 | 74 |

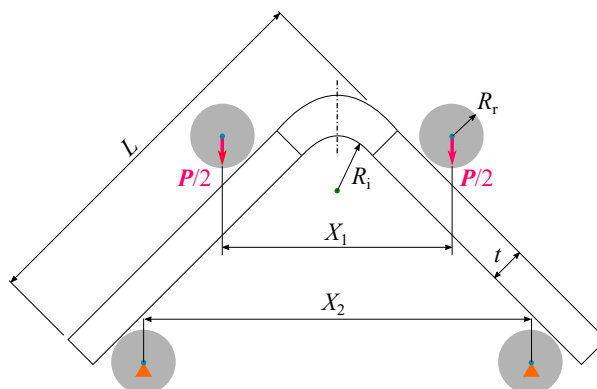


Figure 1. Illustration of the L-shaped clip under four-point bending loading.

2.1. Global model and interface load extraction

In order to have a workflow capable of approximating the global mechanical behaviour of the clip, a simplified global FE model is firstly built to extract the interface loads on the boundaries of the features, using tie constraints to bond the plies. High-fidelity global models using C3D8R solid elements are also built for the purpose of verification, wherein cohesive elements are used between the plies. As shown in Figure 2, the interface loads, consisting with a bending moment M and a force F , transfer information between the global model and the feature model. To reduce the computational cost without loss of accuracy, only half of the specimen is modelled. Since the laminate is highly oriented, it is crucial to apply proper rotationally symmetric boundary conditions [16] for the half model.

To obtain the interface loads F and M from discretised FE models, nodal forces and coordinates are extracted and integrated from all nodes on the section of interest.

2.2. Feature model and failure database generation

Following the proposed workflow, commonly encountered geometric features, such as curved fillets, are identified. A detailed model of the feature at local level is created. For the four-point bending load case, the expected failure mode is Mode I delamination due to interlaminar tensile stress. For the purpose of predicting the critical stress at damage onset, the CZM is used to model the interlaminar interface.

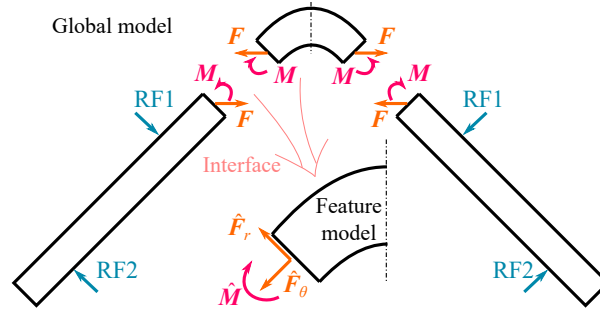


Figure 2. Freebody analysis and illustration of interface loads between global and feature models.

The inclusion of a CZM increases computational cost significantly, thus again to make rational runtime reduction, a half model is built with rotationally symmetric boundary condition applied at the symmetry plane.

The cohesive behaviour is available in Abaqus with damage initiation and evolution models. As shown in Figure 3, the cohesive behaviour used here correlates cohesive tractions in the normal, first shear and second shear directions (σ_n , τ_s and τ_t) with their corresponding separations (δ_n , δ_s and δ_t) through a bilinear constitutive law. The areas under the tractions and their corresponding separations excluding the recoverable energy represent the energy release rate, G_n , G_s and G_t , for each delamination mode [17].

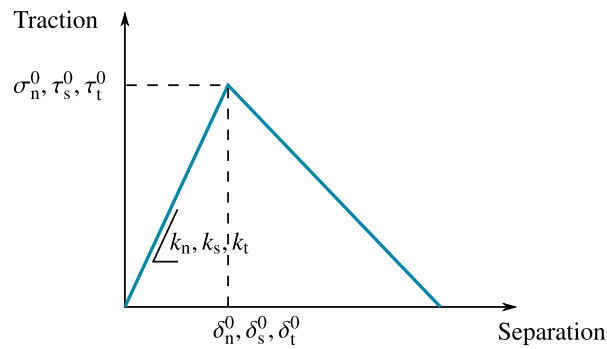


Figure 3. Bilinear traction-separation law.

A quadratic stress-based criterion for damage onset is adopted,

$$f(\boldsymbol{\sigma}) = \left(\frac{\langle \sigma_n \rangle}{\sigma_n^0} \right)^2 + \left(\frac{\tau_s}{\tau_s^0} \right)^2 + \left(\frac{\tau_t}{\tau_t^0} \right)^2 = 1, \quad (1)$$

where $\boldsymbol{\sigma}$ is the stress tensor, σ_n^0 , τ_s^0 and τ_t^0 denote the initial failure stress components in the normal, first shear and second shear directions for each of the single-mode delamination modes I, II and III, respectively. The Macaulay operator, a term which takes the value enclosed by the brackets only when that value is positive, is denoted by brackets $\langle \rangle$. Damage is assumed to initiate when the left-hand side reaches 1, that is $f(\boldsymbol{\sigma}) = f(\sigma_n, \tau_s, \tau_t) = 1$. After damage initiation, there is a reduction in interface stiffness until total fracture of the interface, based on the mixed mode power law for damage evolution,

$$\left(\frac{G_n}{G_n^c} \right)^p + \left(\frac{G_s}{G_s^c} \right)^p + \left(\frac{G_t}{G_t^c} \right)^p = 1, \quad (2)$$

where G_n^c , G_s^c and G_t^c are the critical energy release rate values in the normal, first shear and second shear directions under each of the single-mode delamination modes, and p is the power in the criterion. The interface properties used in cohesive zone modelling are given in Table 3.

Table 3. Interface properties used in cohesive model.

| $k_n = k_s = k_t$ (MPa/mm) | σ_n^0 | τ_s^0 | τ_t^0 | G_n^c | G_s^c | G_t^c | p |
|-------------------------------|--------------|------------|------------|-----------------------|---------|---------|-----|
| | (MPa) | | | (mJ/mm ²) | | | |
| 1×10^7 | 45 | 90 | 90 | 0.2 | 1.2 | 1.2 | 2 |

Unit loads \hat{F}_r , \hat{F}_θ and \hat{M} are applied individually at the interface of the feature model. Although the geometric nonlinearity is included to account for possible large displacements, with the assumption that material constitutive relationship remains linear locally, linear superposition is used to combine the scaled stress and stress resultants, namely,

$$\sigma(\mathbf{M}, \mathbf{F}) = \sigma(k_r \hat{F}_r, k_\theta \hat{F}_\theta, k_M \hat{M}) = k_r \hat{\sigma}_r + k_\theta \hat{\sigma}_\theta + k_M \hat{\sigma}_M, \quad (3)$$

where $\hat{\sigma}_r$, $\hat{\sigma}_\theta$ and $\hat{\sigma}_M$ denote stress responses under individual unit loads \hat{F}_r , \hat{F}_θ and \hat{M} , respectively. Therefore, a failure envelope, which is equivalent to Equation 1, can be established by varying the scale factors k_r , k_θ and k_M in the form of a hypersurface $g(k_r, k_\theta, k_M) = 1$. In this simple case, the *a priori* knowledge from the global model provides an additional constraint for the scale factors, as it is implied in Figure 2: $k_r \hat{F}_r + k_\theta \hat{F}_\theta = \mathbf{F}$. Consequently, the failure surface can be reduced to a 2D envelop. This means by defining $k_F = k_F(k_r, k_\theta)$, it is possible to represent the failure surface as $g(k_F, k_M) = 1$ in a 2D Cartesian system. Nevertheless, in this four-point bending test, the bending moment dominates the mechanical behaviour of the coupon. As a result, the interface force \mathbf{F} contributes far less than the bending moment \mathbf{M} , and has negligible effect to the stress state, as it is shown in Figure 4. Eventually, a 1D failure criterion $g(k_M) = 1$ could be established based on the feature model results. Let $\hat{\sigma}_M$ be the stress response under the unit load \hat{M} , the failure surface can be rewritten as

$$g(k_M) = f(\sigma) = f(k_M \hat{\sigma}_M) = k_M^2 f(\hat{\sigma}_M). \quad (4)$$

Hence, the failure database is made up of only $f(\hat{\sigma}_M)$ that is computed from the feature model.

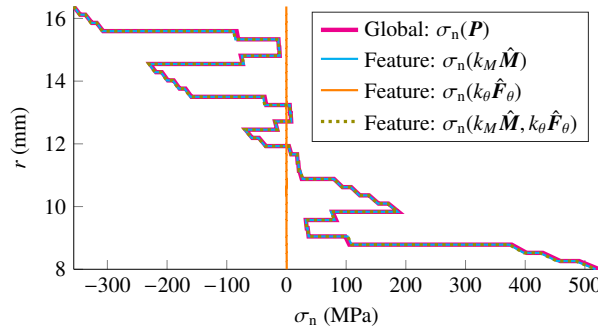


Figure 4. Evaluations of normal stress component σ_n along radial direction r at section of interest under different combination of applied loadings.

2.3. Using the failure database to predict failure initiation and error quantification

As discussed before, the application of a single load (component of \mathbf{M} about the axis of the curved section, or simply denoted by M) is sufficient to replicate the stress state in the region of interest. Therefore,

the current situation may be thought of as a 1D failure problem. In other words, all that is required to be determined is the magnitude of a bending moment M_{Fail} that would initiate failure through delamination. Evaluations of a failure criterion shall be made (in post processing scripts) at multiple points in the region of interest due to some known loading magnitude \hat{M} . The magnitude of this load may then be scaled with k_M such that the peak evaluation of the chosen failure criterion achieves its limit value, namely $g(k_M) = 1$.

Ideally, the local high-fidelity model should be loaded by a bending moment \hat{M} applied to a reference point which is kinematically coupled to the relevant model surface, as described previously. However, directly imposing this kinematic coupling constraint would result in spurious local stress concentrations. To avoid this non-physical effect, a Saint-Venant region is added to the model as shown in Figure 5. This Saint-Venant region is simply an extended section of flat laminate attached to the curved region of interest. The loading reference points is located at the end of this Saint-Venant region, with bending moments defined here as M_{SV} . Note that the magnitude of M_{SV} should be chosen such that the resulting interface moment \hat{M} is unity. Since linear material constitutive behaviour and local linear geometry are assumed, the responses of even modest loads are sufficient to determine failure. In the general case, quasi-unity loads may be applied in all identified directions. The related moment \hat{M} , applied to the interface of the region of interest, may be determined by integrating nodal forces at the interface section. The locations of M_{SV} and \hat{M} may be seen in Figure 5. Nodal stress tensor evaluations are extracted from local models and associated with the applied loads. The failure criterion given in Equation 1 may be evaluated at the lamina interfaces using these stress tensors, noting that σ_n is the stress component normal to the lamina surface while τ_s and τ_t are shear stresses acting on the plane which are orthogonal to this surface. The peak value of the failure criterion may be noted along with its location. The magnitude of this peak failure criterion evaluation is designated here as $f(\hat{\sigma}_M)$. A plot of pointwise (nodal) evaluated failure function $f(\hat{\sigma}_M)$ is presented in Figure 6 under ‘‘application’’ of \hat{M} . By letting $g(k_M) = 1$, the failure bending moment $M_{\text{Fail}} = k_M \hat{M}$ may be determined by solving Equation 4:

$$M_{\text{Fail}} = \hat{M} / \sqrt{f(\hat{\sigma}_M)}. \quad (5)$$

Error can be quantified by comparing with the failure bending moment $M_{\text{Fail}}^{\text{ref}}$ computed from a reference high-fidelity model using the traditional approach, namely

$$\varepsilon = (M_{\text{Fail}} - M_{\text{Fail}}^{\text{ref}}) / M_{\text{Fail}}^{\text{ref}} \times 100\%. \quad (6)$$

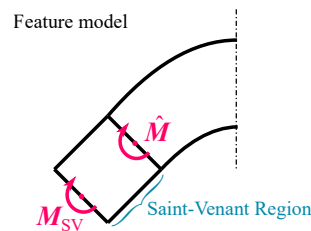


Figure 5. Locations of applied moment M_{SV} and interface moment \hat{M} in feature model.

3. Results and discussions

As a demonstration of the workflow proposed in this work, both global and feature models using approaches with different levels of fidelity were built. Tie constraints and cohesive models are both used to represent the two fidelity levels. The low-fidelity models use tie constraints for interlaminar interfaces to mimic the practical engineering application, while high-fidelity models use cohesive models to provide a reference solution. Two magnitudes of bending moment loads, namely $\hat{M} = 1 \text{ N} \cdot \text{m}$ and $\hat{M} = 100 \text{ N} \cdot \text{m}$,

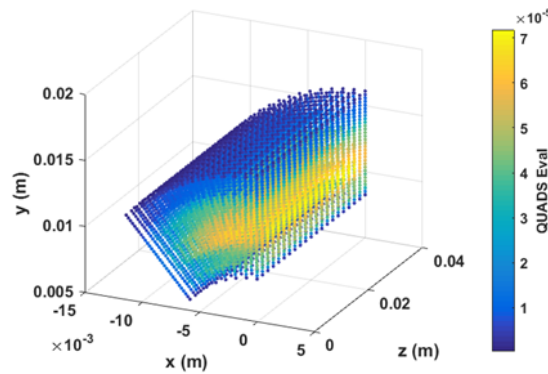


Figure 6. Evaluations of $f(\hat{\sigma}_M)$ at lamina interface nodes for a unit bending moment load application.

have been applied to the feature model to verify the local linearity assumption. Bending moment results and error analysis are reported in Table 4. For the high-fidelity models using CZM, the failure bending moment of global model is $115.8 \text{ N} \cdot \text{m}$ and that of feature model is $108.8 \text{ N} \cdot \text{m}$.

Table 4. Bending moment results and error analysis of the four-point bending clip model.

| Model | \hat{M} ($\text{N} \cdot \text{m}$) | M_{Fail} ($\text{N} \cdot \text{m}$) | Error ε w.r.t. (%) | |
|-------------|--|--|--------------------------------|-----------------|
| | | | Tie Global | Cohesive Global |
| Tie Global | N/A | 119.27 | N/A | 3.00 |
| Tie Feature | 1 | 118.61 | 0.55 | 2.43 |
| | 100 | 120.33 | 0.89 | 3.91 |

From the resulted bending moments, it can be observed that the error caused by different interlaminar interface modelling methods are smaller for the global model while relatively larger for the feature model. Thanks to its lower complexity, the tied interface results in negligible error between global and feature models compared with that of the cohesive interface models.

4. Conclusions and perspectives

A one-way multiscale modelling method is proposed for reusing results of detailed models to identify failure initiation hotspots on global models. Analysis of a simple component has been presented in the present work, namely that of a curved section of laminate loaded in a four point bending configuration. Local high-fidelity models have been developed in order to estimate the onset of delamination in a region of interest (here the curved section of laminate itself).

A brief description of the method implemented in the current work is given, however it must be noted that the adopted procedure can, in principle, be applied to any loading configuration or failure criterion. In more realistic structures it is foreseeable that several internal loads (bending moments and surface tractions applied in convenient coordinate systems which are sympathetic to the local component geometry, combinations of which can be used to approximate any general loading condition experienced by the feature) will be used to generate multidimensional failure envelopes. In this more general case, loading combinations which satisfy the failure criterion would be required. Future work will address this in a more industrially-relevant case by defining a sampling method which estimates such loading combinations.

Acknowledgements

This project is funded by the Clean Sky 2 Joint Undertaking under the European Union's Horizon 2020 research and innovation programme under grant agreement No 754581.

References

- [1] M. J. Hinton, A. S. Kaddour, and P. D. Soden, editors. *Failure Criteria in Fibre Reinforced Polymer Composites: The World-Wide Failure Exercise*. Elsevier, 2004.
- [2] L. Wu, D. Tjahjanto, G. Becker, A. Makradi, A. Jérusalem, and L. Noels. A micro-meso-model of intra-laminar fracture in fiber-reinforced composites based on a discontinuous Galerkin/cohesive zone method. *Engineering Fracture Mechanics*, 104:162–183, May 2013.
- [3] L. Zhao, Y. Gong, J. Zhang, Y. Chen, and B. Fei. Simulation of delamination growth in multidirectional laminates under mode I and mixed mode I/II loadings using cohesive elements. *Composite Structures*, 116:509–522, Sep 2014.
- [4] G. Vigueras, F. Sket, C. Samaniego, L. Wu, L. Noels, D. Tjahjanto, E. Casoni, G. Houzeaux, A. Makradi, J. M. Molina-Aldareguia, M. Vázquez, and A. Jérusalem. An XFEM/CZM implementation for massively parallel simulations of composites fracture. *Composite Structures*, 125:542–557, Jul 2015.
- [5] X. Li and J. Chen. An extended cohesive damage model for simulating multicrack propagation in fibre composites. *Composite Structures*, 143:1–8, May 2016.
- [6] R. Higuchi, T. Okabe, and T. Nagashima. Numerical simulation of progressive damage and failure in composite laminates using XFEM/CZM coupled approach. *Composites Part A: Applied Science and Manufacturing*, 95:197–207, Apr 2017.
- [7] R. Krueger and T. K. O'Brien. Shell/3D modeling technique for the analysis of delaminated composite laminates. *Composites Part A: Applied Science and Manufacturing*, 32(1):25–44, Jan 2001.
- [8] S. Hühne, J. Reinoso, E. Jansen, and R. Rolfes. A two-way loose coupling procedure for investigating the buckling and damage behaviour of stiffened composite panels. *Composite Structures*, 136:513–525, Feb 2016.
- [9] M. Akterskaia, E. Jansen, S. Hühne, and R. Rolfes. Efficient progressive failure analysis of multi-stringer stiffened composite panels through a two-way loose coupling global-local approach. *Composite Structures*, 183(1):137–145, Jan 2018.
- [10] W. Hao, D. Ge, Y. Ma, X. Yao, and Y. Shi. Experimental investigation on deformation and strength of carbon/epoxy laminated curved beams. *Polymer Testing*, 31(4):520–526, Jun 2012.
- [11] G. Seon, A. Makeev, Y. Nikishkov, and E. Lee. Effects of defects on interlaminar tensile fatigue behavior of carbon/epoxy composites. *Composites Science and Technology*, 89:194–201, Dec 2013.
- [12] A. Makeev, G. Seon, Y. Nikishkov, and E. Lee. Methods for assessment of interlaminar tensile strength of composite materials. *Journal of Composite Materials*, 49(7):783–794, Mar 2015.
- [13] J.-S. Charrier, F. Laurin, N. Carrere, and S. Mahdi. Determination of the out-of-plane tensile strength using four-point bending tests on laminated L-angle specimens with different stacking sequences and total thicknesses. *Composites Part A: Applied Science and Manufacturing*, 81:243–253, Feb 2016.
- [14] K. H. Nguyen, H. W. Ju, V. H. Truong, and J. H. Kweon. Delamination analysis of multi-angle composite curved beams using an out-of-autoclave material. *Composite Structures*, 183(1):320–330, Jan 2017.
- [15] ASTM International. *D6415/D6415M-06a(2013) Standard Test Method for Measuring the Curved Beam Strength of a Fiber-Reinforced Polymer-Matrix Composite*. West Conshohocken, PA, 2013.
- [16] S. Li and S.R. Reid. On the symmetry conditions for laminated fibre-reinforced composite structures. *International Journal of Solids and Structures*, 29(23):2867 – 2880, 1992.
- [17] E. J. Barbero. *Finite Element Analysis of Composite Materials using Abaqus*. CRC Press, 2013.